

## Journal Pre-proofs

Novel antibody-drug conjugate with UV-controlled cleavage mechanism for cytotoxin release

Jiaguo Li, Dian Xiao, Fei Xie, Wei Li, Lei Zhao, Wei Sun, Xiaohong Yang, Xinbo Zhou

PII: S0045-2068(20)31773-9  
DOI: <https://doi.org/10.1016/j.bioorg.2020.104475>  
Reference: YBIOO 104475

To appear in: *Bioorganic Chemistry*

Received Date: 25 July 2020  
Revised Date: 9 November 2020  
Accepted Date: 11 November 2020

Please cite this article as: J. Li, D. Xiao, F. Xie, W. Li, L. Zhao, W. Sun, X. Yang, X. Zhou, Novel antibody-drug conjugate with UV-controlled cleavage mechanism for cytotoxin release, *Bioorganic Chemistry* (2020), doi: <https://doi.org/10.1016/j.bioorg.2020.104475>

This is a PDF file of an article that has undergone enhancements after acceptance, such as the addition of a cover page and metadata, and formatting for readability, but it is not yet the definitive version of record. This version will undergo additional copyediting, typesetting and review before it is published in its final form, but we are providing this version to give early visibility of the article. Please note that, during the production process, errors may be discovered which could affect the content, and all legal disclaimers that apply to the journal pertain.

© 2020 Published by Elsevier Inc.



Article

# Novel antibody-drug conjugate with UV-controlled cleavage mechanism for cytotoxin release

Jiaguo Li<sup>1,2,‡</sup>, Dian Xiao<sup>2,‡</sup>, Fei Xie<sup>2</sup>, Wei Li<sup>2</sup>, Lei Zhao<sup>2</sup>, Wei Sun<sup>1,\*</sup>, Xiaohong Yang<sup>1,\*</sup>, and Xinbo Zhou<sup>2,\*</sup>

<sup>1</sup> School of Pharmaceutical Sciences, Jilin University, Changchun 130021, China;

<sup>2</sup> National Engineering Research Center for the Emergency Drug, Beijing Institute of Pharmacology and Toxicology, Beijing 100850, China; li\_jiaguo@126.com (J.L.); be\_xiaodian@163.com (D.X.); xiefei0058@163.com (F.X.); a\_moon1096@163.com (W.L.); leizhao-hit@hotmail.com (L.Z.);

<sup>‡</sup> These authors contribute equally to this work

\* Correspondence: wsun@jlu.edu.cn (W.S.); xiaohongyang88@126.com (X.Y.); zhouxinbo@bmi.ac.cn (X.Z.); Tel.: +86-010-6693-0674 (X.Z.)

Received: date; Accepted: date; Published: date

**Abstract:** Antibody-drug conjugates (ADCs) are being developed worldwide with the potential to revolutionize current cancer treatment strategies. However, off-target toxicity caused by the instability of linkers remains one of the main issues to be resolved. Developing a novel photocontrol-ADC with good stability and photocontrolled release seemed to be an attractive and practical solution. In this study, we designed, for the first time, a novel ultraviolet (UV) light-controlled ADC by carefully integrating the UV-cleavable *o*-nitro-benzyl structure into the linker. Our preliminary work indicated that the ADC exhibited good stability and photocontrollability while maintaining a targeting effect similar to that of the naked antibody. Upon irradiation with UV light, the ADC rapidly released free cytotoxins and exerted significant cytotoxicity toward drug-resistant tumor cells. Compared to those of the unirradiated cells, the EC<sub>50</sub> values of ADCs increased by up to 50-fold. Furthermore, our research confirmed that the degradation products of unirradiated ADC, Cys-1a, were relatively less toxic, thus potentially reducing the off-target toxicity caused by nonspecific uptake of ADCs. The novel design strategy of UV light-controlled ADCs may provide new perspectives for future research on ADCs and promote the development of photocontrol systems.

**Keywords:** antibody-drug conjugate; photocontrol; ultraviolet radiation; *o*-nitro-benzyl;

## 1. Introduction

In recent years, antibody-drug conjugates (ADCs) have been developed worldwide with the potential to revolutionize current cancer treatment strategies<sup>1-3</sup>. Structurally, they are formed through conjugation of an antibody to a highly active cytotoxin via a linker. Currently, nine ADCs have been approved, and more than 80 are at different phases of clinical trials<sup>4,5</sup>.

Essentially, as a prodrug, ADCs are ideally highly stable in the circulatory system and release cytotoxins in the tumor microenvironment. Therefore, the linker, similar to the trigger of the ADC, is always the key in ADC design<sup>6-8</sup>. To date, three generations of ADCs have been developed: first-generation ADCs that contain acid-labile linkers, such as hydrazone and carbonate bonds, represented by the drugs Mylotarg<sup>9</sup> and Besponsa<sup>10</sup>; and second- and third-generation ADCs that predominantly contain enzyme-cleavable linkers, such as Adcetris<sup>11</sup>. Although the continuous development of ADCs has effectively improved their therapeutic index to a certain extent, off-target toxicity caused by the instability of linkers remains one of the main issues to be resolved. For example, mainstream enzyme-cleavable ADCs mainly utilize cathepsin, which is present in all mammalian tissue cells for drug release<sup>12</sup>, but the degradation behaviors of off-target ADC linker structures can lead to toxic events, thereby limiting their further clinical applications (Figure 1a). A study has shown that more than 23 of the 55 conventional ADCs fail because of poor therapeutic indexes<sup>5</sup>. Therefore, the development of linker technology with a novel drug release mechanism is urgently needed.

In recent years, photocontrol technology has been widely studied as a noninvasive approach, which allows control of active substance release with high spatiotemporal precision<sup>13-17</sup>. The principle behind this technology is that a photoremovable protecting group (PPG) is linked to an active drug via a covalent bond to mask its activity. However, the bond can be cleaved by external irradiation to release the active component from the



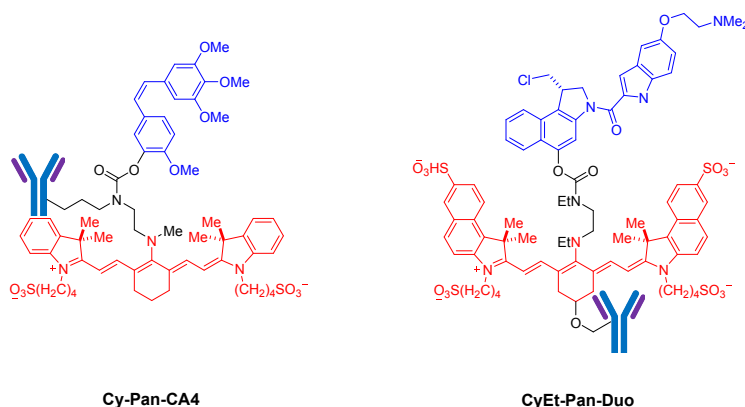


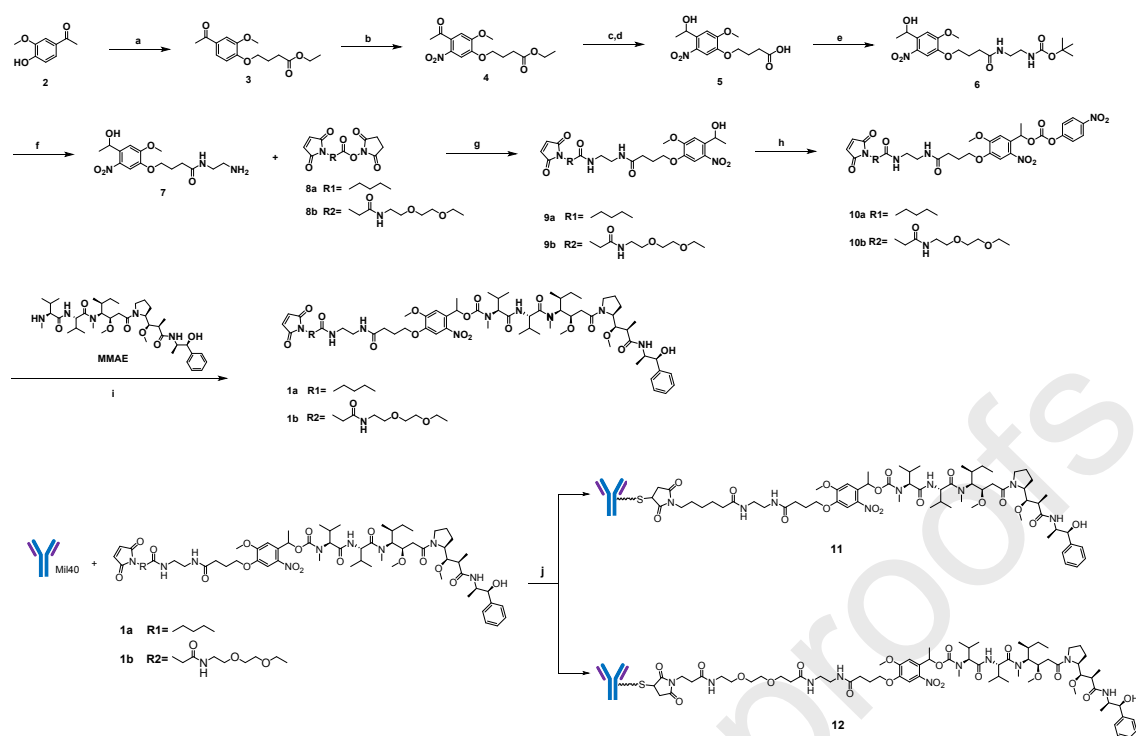
**Figure 2.** Structure of two near-infrared light activated ADCs that have been reported.

Herein, we report, for the first time, a type of ADC that utilizes ultraviolet (UV) light to achieve photocontrolled drug release. In this design, we carefully introduced a UV light-controlled *o*-nitrobenzyl group to replace the *p*-aminobenzyl (PAB) in linkers. In addition, this would help to maximize maintaining the optimum pharmacological properties of ADCs (Figure 1b). Currently, the *o*-nitrobenzyl system and its derivatives are among the most commonly used photosensitive protective groups (PPGs) in biological research<sup>22-25</sup>, and some studies have shown that these PPGs have almost no cytotoxicity after photolysis<sup>26,27</sup>. Our novel type of ADC can be delivered to tumor sites by utilizing the targeting function of the antibody. Upon brief UV irradiation, the *o*-nitrobenzyl group formed a highly active diradical, followed by dehydrogenation of the carbon atom in the  $\gamma$ -position<sup>25-27</sup>, after which the cytotoxic drug was cleaved and released (Figure 1B). 1b), finally achieving precise temporal and spatial control. In this study, we synthesized an ADC using the highly active cytotoxic drug monomethyl auristatin E (MMAE) ( $EC_{50} = 0.18$  nM) and the well-studied antibody mil40, which is a biosimilar of trastuzumab and is in the clinical research stage (CTR20180362)<sup>28-30</sup>. Our preliminary work revealed that our ADC possessed some promising features, such as good stability and targeting effect. In addition, it rapidly released drugs and effectively destroyed drug-resistant breast and gastric cancer cells only after irradiation with UV light. Our work presented herein preliminarily validated the feasibility of photocontrolled ADCs for achieving drug release upon UV light irradiation. The novel design strategy of UV light-controlled ADCs may provide new perspectives for future research on ADCs and promote the development of photocontrol systems.

## 2. Results and Discussion

### 2.1. Chemistry

As shown in Scheme 1, the linker-MMAE portion, i.e., compounds **1a** and **1b**, was first synthesized, and 4-Hydroxy-3-methoxyacetophenone and ethyl 4-bromobutyrate were used as starting materials. The substitution reaction was performed under the catalysis of potassium carbonate at 50°C to obtain compound **3**, followed by a nitration reaction in acetic anhydride and nitric acid to obtain compound **4**. Compound **5** was obtained by a two-step reaction: compound **4** was hydrolyzed in a hot acidic solution of acetate and water, and the ketone of the resulting intermediate was further reduced to a hydroxyl group by NaBH<sub>4</sub> to produce compound **5**. Compound **6** was obtained via a condensation reaction between Boc-protected ethylenediamine and compound **5**. Compound **7** was obtained after removal of the Boc group in an acidic environment. The naked amino groups were reacted with the respective chain structures that had different maleimide-containing linkers (**8a** and **8b**) to produce bifunctional linkers **9a** and **9b**. The bifunctional linkers were reacted with bis(*p* nitrophenyl) carbonate on one end to produce active intermediates **10a** and **10b**, and these were further conjugated with the toxin MMAE to obtain compounds **1a** and **1b**.



**Scheme 1.** Synthesis of ADC **11** and **12**. Reagents: (a) anhydrous DMF,  $K_2CO_3$ , Ethyl 4-bromobutyrate,  $50^\circ C$ , 6 h; (b)  $HNO_3$ ,  $Ac_2O$ ,  $0^\circ C$ , 5 h, (c)  $HCl$ ,  $H_2O$ ,  $AcOH$ , reflux, 1 h, (d)  $NaBH_4$ ,  $EtOH$ ,  $NaHCO_3$ , (e) tert-butyl(2-aminoethyl)carbamate, EDCI, HOBT, DIPEA, DMF, r.t., overnight, (f)  $HCl$ , r.t., 3 h, (g) DIPEA, anhydrous DMF, r.t., overnight, (h) bis(4-nitrophenyl)carbonate, anhydrous DMF, DIPEA, r.t., overnight, (i) anhydrous DMF, HOBT, DIPEA, r.t., 12 h. (j) monoclonal antibody (Mil40), TECP, NAC,  $H_2O$ , r.t.

## 2.2. Conjugation to antibody

Compounds **1a** and **1b** were each conjugated to an antibody to produce ADCs. To expedite our targeted studies, we selected the well-studied humanized monoclonal antibody mil40 that targets HER2, which is a marketed biosimilar of Herceptin. The intermolecular disulfide bond of the mil40 antibody was reduced by TECP to free the sulfhydryl groups, the position of which enabled the linkage of the maleimide-containing compounds **1a** and **1b**. The reaction was terminated by NAC. Finally, ADCs **11** and **12** were obtained (Scheme 1).

## 2.3. In vitro characterization

After conjugating the antibody to the novel linker-MMAE described above, we performed quality control work to characterize ADC **11** and ADC **12**. Hydrophobic interaction chromatography (HIC) analysis of the two ADCs allowed resolution of the conjugates into several major peaks corresponding to 0, 1, 2, 3, 4, 5 and 6 drug molecules per antibody (Figure 3a), with an average DAR of approximately 3.4 and 2.6 for ADC **11** and **12**, respectively. The proportion of unconjugated naked antibodies was less than 10%, and was 4.1% and 9.7% for ADC **11** and ADC **12**, respectively. At the same time, liquid chromatography-mass spectrometry (UPLC-Q-TOF-MS) analysis of native ADCs showed that ADCs **11** and **12** contained 2.7 drugs per antibody (Figure 3a). The DAR value was slightly lower than that detected by HIC, which might be due to the inhibition of ionization signal by the conjugated linker payloads. According to size exclusion chromatography (SEC) analysis, ADCs **11** and **12** were composed nearly exclusively (>98.5% purity) of single monomeric species (Figure 3a).

The stability of new UV-controlled linkers in the circulatory system is a critical factor in determining the efficacy and toxicity of ADCs. Therefore, we tested herein the stability of the linker-MMAE in human serum. ADCs **11** and **12** were incubated in 50% human plasma at  $37^\circ C$ , and the amount of released MMAE was monitored by LC-MS. The standard curve of MMAE revealed that the linear range of MMAE was 0.25 nM to 250 nM (Figure 3b). It has been calculated that approximately 3.28 nM and 1.87 nM MMAE were released from 100 nM of ADCs **11** and **12**. In other words, less than 1% of the total MMAE (approximately 340 nM for

ADC 11 and 240 nM for ADC 12) was released during 6 days in human plasma (Figure 3b). This result suggested that the new UV-controlled linkers were very stable in human plasma.

Under normal conditions, degradation of ADCs in lysosomes will release the structural components of conjugates containing amino acid residues of the antibody, linkers, and cytotoxins<sup>31-33</sup>, such as compounds Cys-**1a** and Cys-**1b** (Figure 1b). To mimic these structures, we reduced the reactive maleimide double bonds of **1a** and **1b** with an excess of L-cysteine to obtain Cys-**1a** and Cys-**1b**, respectively. These compounds were mixed with PBS buffer and incubated at 37°C for seven days. Aliquots were collected at different time points prior to HPLC analysis and then stored at -80°C. The peak areas of the compounds at each time point were plotted against the sampling time (Figure 3c). The results showed that there were no significant changes in the peak areas of the two compounds after seven days. This indicated that our linker-MMAE did not break, that no cytotoxins were released and that the compounds had good stability in PBS.

We next investigated whether the antibody in the ADC retains its original antigen-binding capacity at the protein and cellular levels. We first performed an enzyme-linked immunosorbent assay (ELISA) on ADCs **11** and **12** to assess their affinities for the HER2 protein. The results showed that the EC<sub>50</sub> values of ADC **11** and **12** were 0.015 nM and 0.017 nM, respectively, which were similar to that of naked antibody mil40 (EC<sub>50</sub> = 0.007 nM) (Figure 3d). This indicated that there was no discernable effect on the affinity of the antibody toward HER2 after conjugation.

In addition to satisfying the condition of stability in the circulatory system, the linker must be capable of rapidly and efficiently releasing cytotoxic compounds at the target tissue to achieve the function of destroying tumor cells. Therefore, we next investigated the photorelease kinetics of compounds **1a** and **1b**. Studies have shown that wavelengths shorter than 300 nm may cause damage to tissues and proteins. In contrast, UV irradiation with wavelengths longer than 320 nm results in less DNA damage and is harmless at low doses<sup>34, 35</sup>. In line with this concept, we performed our experiments using a UV crosslinker that emitted a wavelength of 365 nm (40 W), which has been shown to be capable of cleaving PPG 4,5-dimethoxy- 2-nitrobenzyl (DMNB). We irradiated 40 µM solutions of compounds **1a** and **1b** in methanol, and the cytotoxin release results are shown in Figure 3e. Upon irradiation, both compounds showed a rapid release of MMAE that reached the highest platform within 10 min. In addition, this photocleavage experiment could also serve as a reference for determining irradiation time in subsequent cell cytotoxicity experiments.

In general, the released small molecule cytotoxins also require sufficient stability at the used wavelength of UV light. Otherwise, the cytotoxins would be degraded immediately after its release or even before the bond to the PPG is cleaved. We next evaluated the UV stability of the MMAE. MMAE solutions (1 mg/ml) in methanol were irradiated at 365 nm (40 W). Under these conditions, MMAE showed excellent stability within 30 minutes (Supplementary Figure S1).

#### 2.4 Cell binding and endocytosis

At the cellular level, in view of the HER2-targeting property of the antibody, we selected BT474 breast cancer cells that expressed high levels of HER2 for flow cytometry experiments to evaluate the binding of compounds to the cell-surface HER2 antigen. We found that the mean fluorescence intensity signals in the experimental group, in which ADCs **11** and **12** were added, were much higher than those in the blank control cell group and were similar to those obtained with naked antibody mil40. However, in the negative control MCF-7 cells, which had low HER2 expression, the average fluorescence intensity did not significantly increase after the addition of naked antibody mil40 and compounds (Figure 4a). These results indicated that ADCs **11** and **12** specifically bound to the HER2 antigen on the surface of BT474 cells. In addition, the results of confocal microscopy showed that cells incubated with the green fluorescence-stained ADC **12** and naked antibody mil40 at 30 min at 4°C displayed a similar pattern, where they were bound to the HER2 antigen on the surface of the BT474 cell membrane. After incubation at 37°C for 24 h, scattered staining was observed within the cells, and the intracellular signals colocalized with that of lysosomes appeared yellow, indicating that ADC **12** was internalized and transported to the lysosomes (Figure 4b).

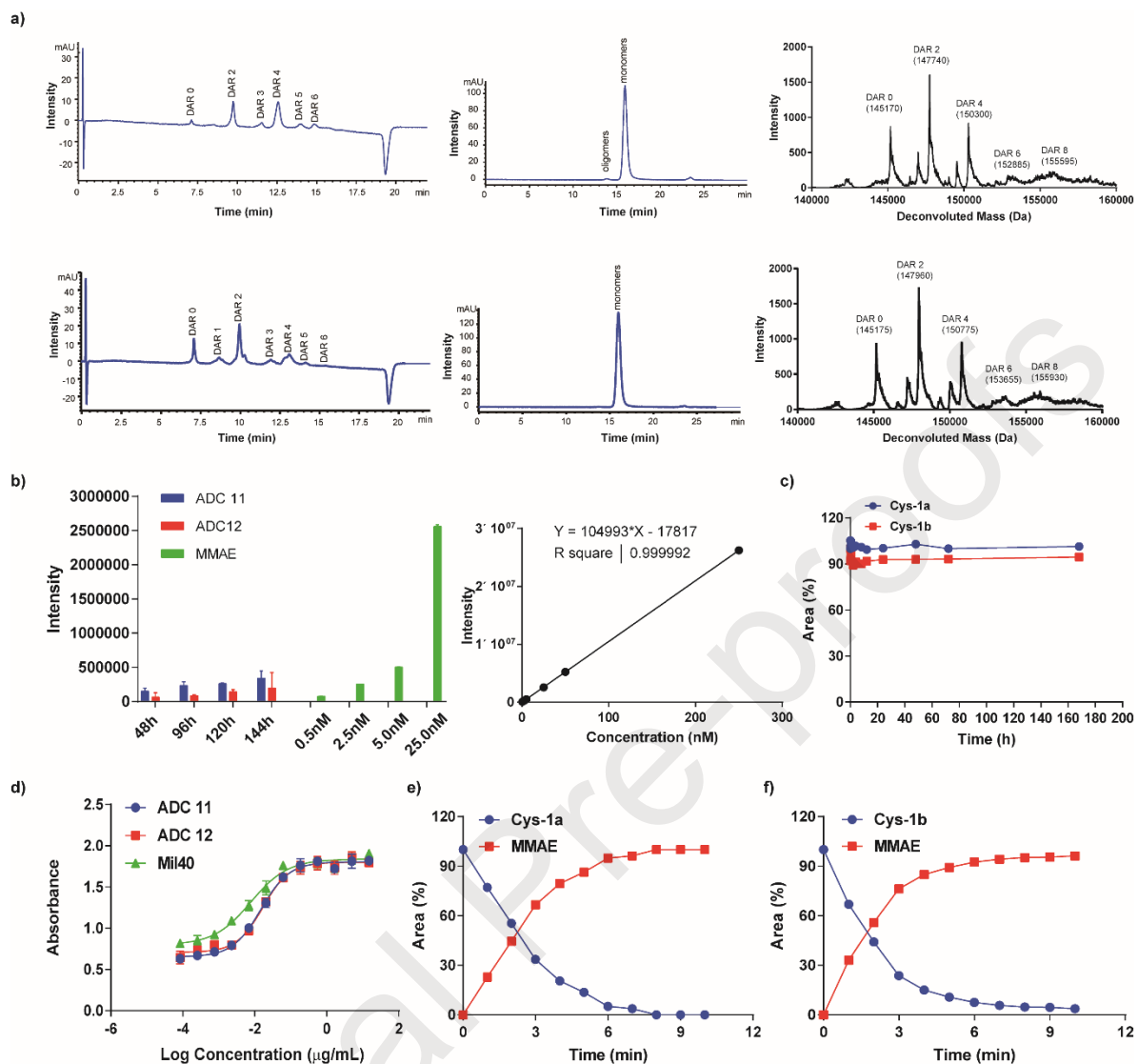


**Figure 3** *In vitro* characterization of novel UV-controlled linkers and ADCs. (a) HIC, SEC and UPLC-Q-TOF-MS assays of ADC 11 and 12. (b) Stability assays of linker-MMAE. ADC 11 and 12 were incubated in 50% human plasma at 37 °C for seven days and analyzed by LC-MS. (c) Stability assays of linker-MMAE. Compounds Cys-1a and Cys-1b in pH = 7.4 PBS were incubated at 37 °C for seven days and analyzed by HPLC. (d) Affinity tests of ADC for HER2 protein by ELISA.  $EC_{50}$  value of mil40 was 0.007 nM,  $EC_{50}$  value of ADC 11 and 12 was 0.015 and 0.017 nM. (e) and (f) UV-cleavage tests on the linker-MMAE. 40  $\mu\text{M}$  compound solutions in methanol were irradiated at 365 nm for 10 min and analyzed by HPLC.

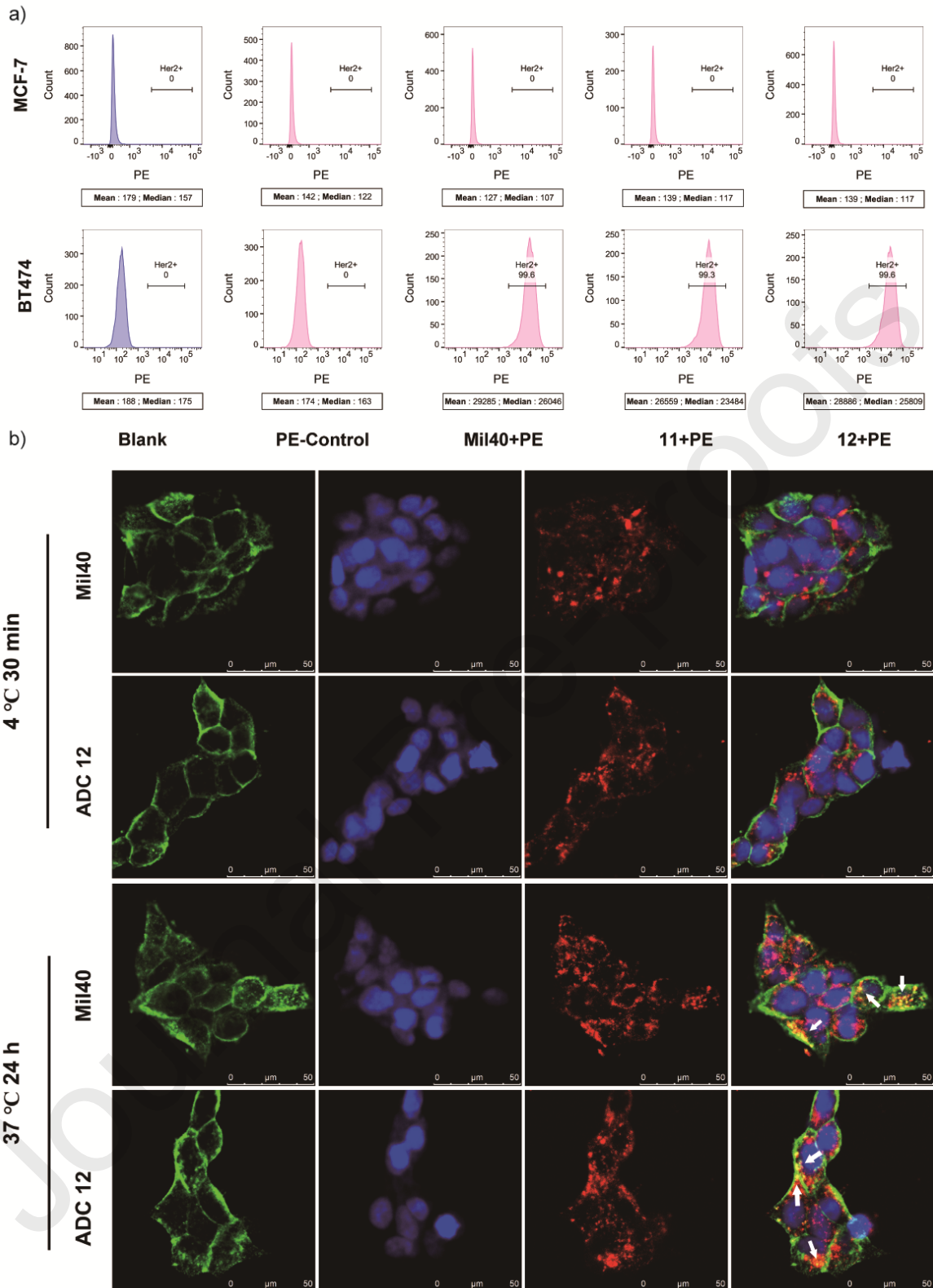


**Figure 4.** Cell binding and endocytosis of the novel UV-controlled ADCs. (a) The ability of ADC **11** and **12** to bind to the highly expressed HER2 antigen on BT474 cell membrane was examined by flow cytometry. MCF-7 cells with low expression of HER2 antigen on cell membrane as negative control. (b) Traffic of positive control antibody mil40 or ADC **12** to lysosome in BT474 cells visualized by confocal microscopy. Mil40 or ADC **12** stained by Alexa 48-labeled second antibody was shown in green, DAPI-stained nuclei was shown in blue, lysosome markers CD107b stained by Alexa Fluor 647-labeled anti-human CD107b antibody was shown in red. Co-localization of signals for mil40 or ADC **12** with lysosome markers was shown as yellow. Magnification bar, 50  $\mu\text{m}$ .

## 2.5. Cytotoxicity of ADCs with or without UV irradiation

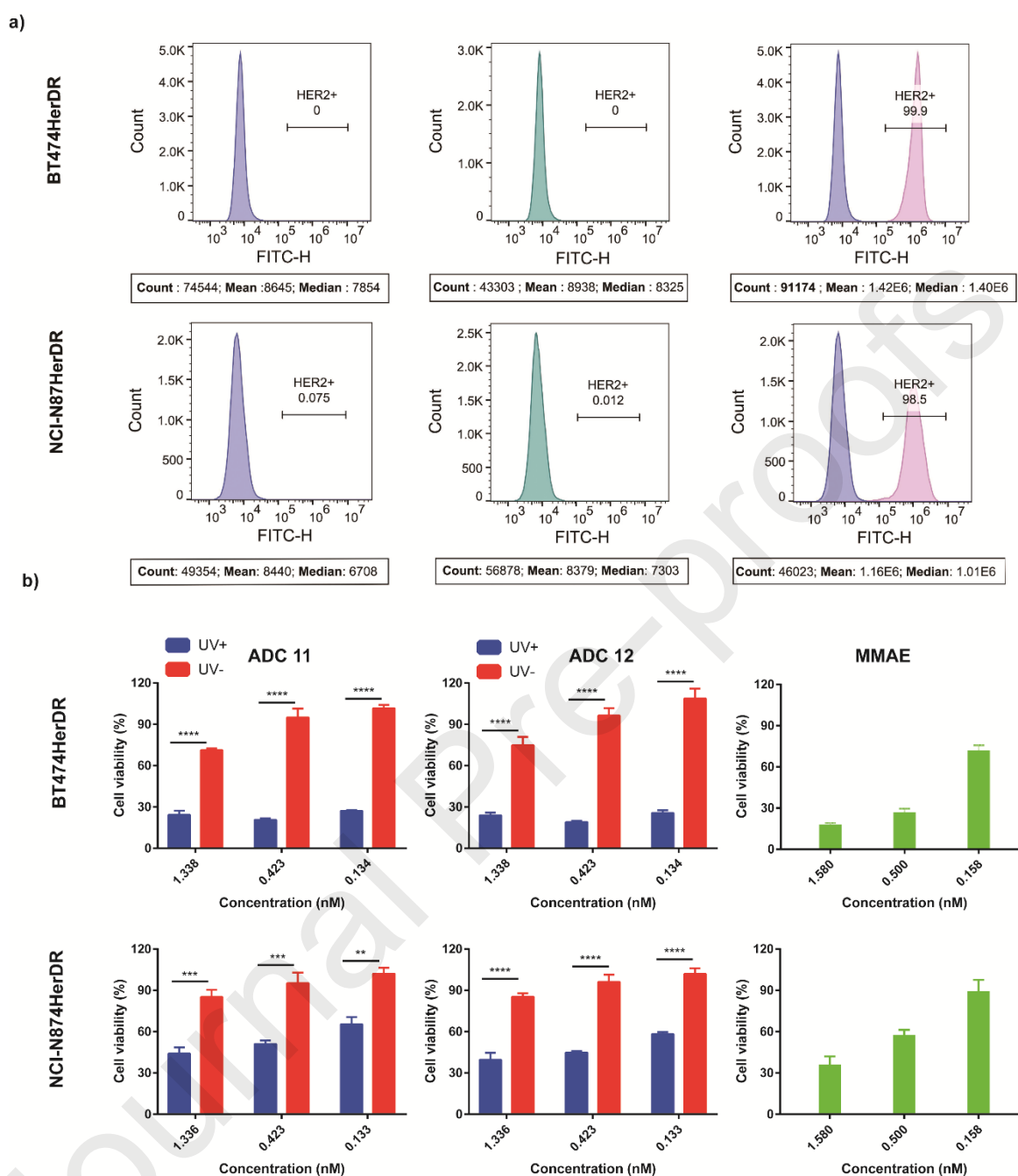


**Figure 5.** Her2 expression and Cytotoxicity. (a) Her2 expression was tested in two Herceptin-resistant cell lines. Cells not stained with FITC was shown in purple peaks, isotype control-FITC was shown in green peaks, anti-Her2 Ab-FITC was shown in pink peaks. (b) Cytotoxicity of ADCs with or without UV irradiation. Two-way ANOVA analysis, \*  $p < 0.05$ , \*\*  $p < 0.01$ , \*\*\*  $p < 0.001$ , \*\*\*\*  $p < 0.0001$ .

In view of the good stability and photocleavability of the linker-MMAE payload, as well as the fact that ADC possessed an antigen-binding capacity similar to that of a naked antibody, we next verified the feasibility of the design strategy for UV light-controlled ADCs through cell proliferation experiments. Regarding cell line selection, we considered that the mil40 monoclonal antibody could exhibit the same tumor cell-killing effect as Herceptin. Therefore, we herein utilized the Herceptin-resistant cell lines BT474-HerDR and N87-HerDR, which can block the action of this antibody, to objectively assess the true toxicity of the novel linker MMAE after irradiation. We first verified the expression of HER2 antigen in these two cell lines using flow cytometry. The results showed that nearly 100% of the cells were HER2-positive. In addition, the fluorescence signals were intense, suggesting a high abundance of HER2 expression in each cell (Figure 5a).

After incubation with ADCs **11** and **12** for 2 h, the cells were irradiated with UV light at 365 nm (40 W), and a cell growth assay was performed. The irradiation time of the cells could be selected based on the photocleavage experiment to allow sufficient release of cytotoxins after UV irradiation; however, the timing in which the cells could tolerate UV light must also be considered. We conducted relevant experiments and determined that the longest UV irradiation time tolerated by BT474-HerDR cells was 3 min (Supplementary Figure S2). First, we found that without UV irradiation, the activity of ADCs declined more than 10 times more than MMAE. This may indicate that off-target toxicity caused by nonspecific uptake of ADC was significantly reduced. Furthermore, it was exciting to find that the activities of ADC **11** ( $EC_{50} = 0.04$  nM) and **12** ( $EC_{50} = 0.04$  nM) were greatly increased after 3 min of UV irradiation. Compared to those of the unirradiated compounds, the  $EC_{50}$  values increased by 50-fold, and the inhibition rates were significantly higher under UV irradiation than those of the unirradiated compounds ( $p < 0.0001$ , Figure 5b, Table 1). We also performed the same tests on N87-HerDR cells and determined that the irradiation time for N87-HerDR cells was 5 min. After UV irradiation, the  $EC_{50}$  values of ADC **11** and **12** were 0.24 nM and 0.23 nM, respectively, which were approximately 15-fold higher than those of unirradiated cells (Table 1). Similarly, we found that the inhibition rate was significantly higher under UV irradiation than without ( $p < 0.01$ , Figure 5b, Table 1). Nontargeted effects of ADC **11** and **12** were assessed on MCF7 breast cancer lines lacking HER2 expression. Both ADCs tested showed minimal antiproliferative activity in MCF7 cells with  $EC_{50}$  values of 88.64 nM and 45.10 nM, respectively, whereas free MMAE showed potency equal to that observed on the HER2-positive lines (Table 1). The cytotoxicity of ADC **11** and **12** on HER2-negative cells was more than 100-fold lower than that on HER2-positive cells. These results indicated that our ADCs exhibited good UV controllability and antigen selectivity, the off-target toxicity was greatly reduced without UV irradiation and the tumor cell-killing effects were rapidly activated after a short UV irradiation.

**Table 1.** Cell proliferation inhibition activities of two ADCs with or without UV irradiation in two Herceptin-resistant cell lines and Herceptin-negative cell lines.

Test compound	BT474-HerDR Cell	BT474-Ratio	N87-HerDR Cell	N87-Ratio	MCF 7 Cell
	$EC_{50}$ (nM)	(UV-/UV+)	$EC_{50}$ (nM)	(UV-/UV+)	$EC_{50}$ (nM)
mil40	7316.59	—	9668.35	—	>666.67
MMAE	0.18	—	0.45	—	0.64
<b>11</b> (UV-)	2.03		3.55		
<b>11</b> (UV+)	0.04	50.75	0.24	14.79	88.64
<b>12</b> (UV-)	2.17		3.95		
<b>12</b> (UV+)	0.04	54.25	0.23	17.17	45.10

Radiation by UVP Crosslinker (360nm, 40W). BT474-HerDR cells was irradiated for 3min, N87-HerDR Cells was irradiated for 5min.

## 2.6. Off-target toxicity of ADCs

An interesting observation was that unirradiated ADCs **11** and **12** exhibited less cytotoxicities than MMAE. In fact, when ADCs were not exposed to UV light, they might be endocytosed (Figure 4) and degraded by the lysosomes into Cys-**1a** and Cys-**1b** (Figure 6a). In our latest research, we detected Cys-linker-MMAE as one of the degradation products from ADCs in cells by LC-MS/MS<sup>36</sup>. Therefore, we speculated that the two degradation products may be less toxic. The advantage of the low toxicity of the degradation products was the reduction of the toxic adverse effects of the ADCs because of early degradation in the circulation or nonspecific uptake. Thus, we first tested the cell proliferation inhibition activities of Cys-**1a** and Cys-**1b**. The results indicated that compared with MMAE in the three cells, the cytotoxicity of Cys-**1a** and Cys-**1b** obviously decreased, with a maximum reduction of approximately 47 times (Figure 6b). It was exciting to find that the unirradiated Cys-**1a** and Cys-**1b** exhibited less cytotoxicity to N87-HerDR cells and BT474-HerDR cells, with

EC<sub>50</sub> values similar to those of ADC **11** and ADC **12**. This outcome primarily achieved our design goal of reducing off-target toxicity by a low-toxicity prodrug form, Cys-linker-MMAE (Figure 6b).

Moreover, the lipid-water partition coefficient, MlogP, of Cys-**1a** and Cys-**1b** predicted by ADMET predictor 8.0 software was -2.624 and -4.336, respectively (Table 2). Compared with MMAE (1.911), a remarkable reduction was observed. Other permeability parameters such as S + MDCK exhibited the same downward trend (Table 2). These experimental results indicated that the decline in the permeability of Cys-linker-MMAE contributed to the reduction of cytotoxicity and a lower bystander effect.

Next, tubulin polymerization assays were performed on these two compounds to analyze further the reason underlying the reduced toxicity. Both Cys-**1a** and Cys-**1b** exhibited a concentration-dependent inhibition of tubulin polymerization (Figure 6c), and the calculated EC<sub>50</sub> was 6.28 μM and 7.17 μM, respectively. Compared with that of MMAE, their inhibitory effects were reduced by 6- and 7-fold, respectively (Table 2), confirming that the compounds exhibited lower toxicities than MMAE. Comprehensive results of tubulin polymerization assays and cytotoxic experiments indicated that the compound Cys-**1a** could be used as a good lead compound to provide a structural basis for subsequent optimization to further reduce the toxicity of degradation products.

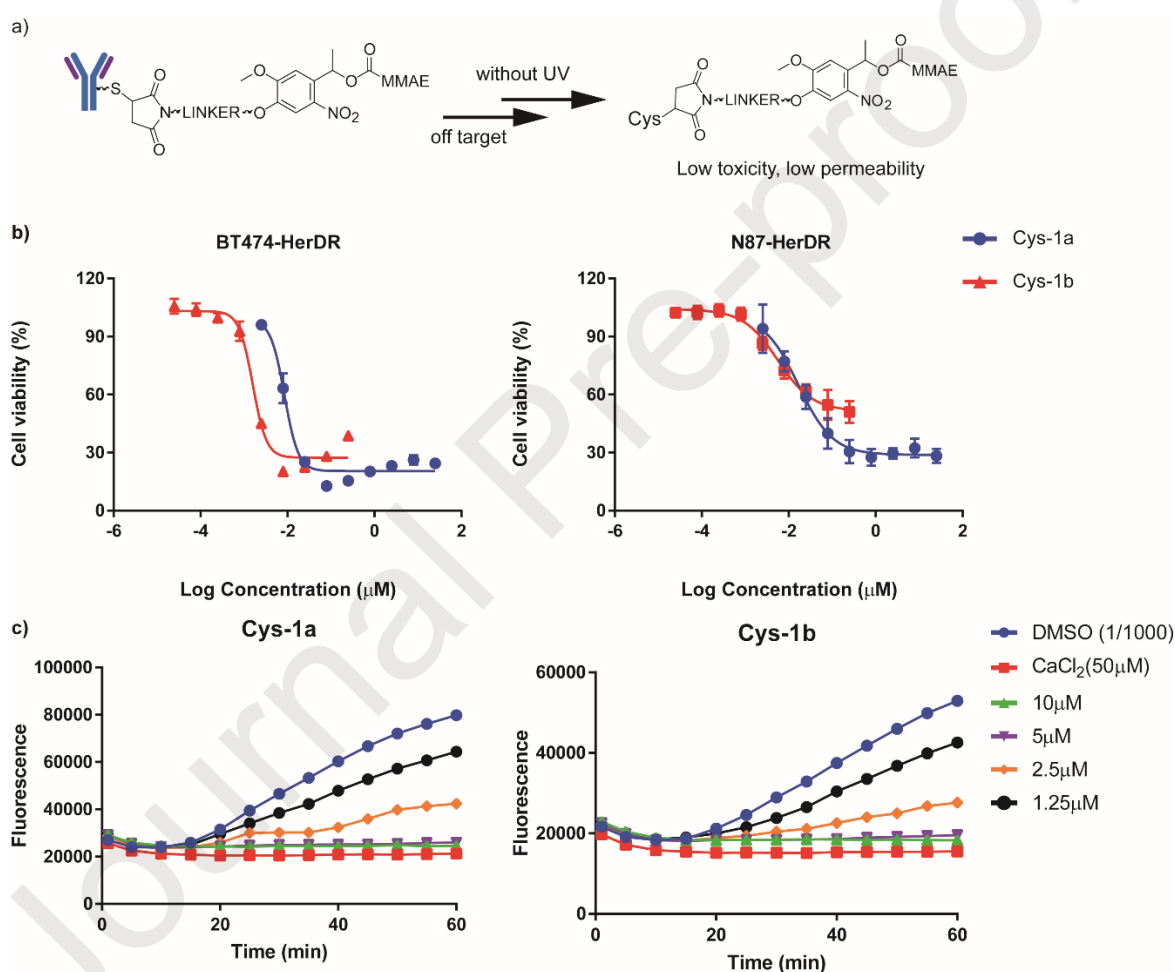


**Figure 6.** Off-target toxicity of ADCs. (a) ADCs were degraded into Cys-**1a** and Cys-**1b** without UV. (b) Effect of Cys-**1a** and Cys-**1b** on tubulin polymerization *in vitro*. Purified tubulin protein at 2 mg/mL in a reaction buffer was incubated at 37 °C in the presence of 0.1% DMSO, test compounds at 1.25, 2.5, 5, or 10 μM. Polymerizations were followed by an increase in fluorescence emission at 460 nm over a 60 min period at 37 °C.

**Table 2.** Inhibitory activity of Cys-**1a** and Cys-**1b** on Tubulin Polymerization

Test compound	MlogP <sup>a</sup>	S+MDCK <sup>b</sup>	BT474-HerDR Cell	N87-HerDR Cell	Inhibition of tubulin polymerization
			EC <sub>50</sub> (nM)	EC <sub>50</sub> (nM)	EC <sub>50</sub> (μM)
MMAE	1.191	21.818	0.18	0.45	1.11

Cys-1a	-2.624	4.34	8.53	16.54	6.28
Cys-1b	-4.336	4.303	1.59	5.62	7.17

<sup>a</sup> MlogP: Oil-water partition coefficient of compounds. Higher value indicates a better fat solubility. <sup>b</sup> S+MDCK: Used to predict the apparent permeability coefficient of compounds in Madin-Darby canine kidney cell models. Higher values indicate greater membrane permeability.

### 2.7. *In vivo* imaging of fluorescein-labeled ADC

The *in vivo* distribution and tumor targeting ability of Mil40 and ADC **11** were evaluated in a BALB/c nude mouse NCI-N87 xenograft model by an optical imaging system. We used DyLight 680 NHS ester-labeled Mil40 and ADC **11** to administer the tail vein of mice at a dose of 20 mg/kg, and the intense fluorescence signal in the tumor site was clearly visualized within 6 h. Subsequently, the tumor-located image was clearly maintained for approximately 15 days, and eventually the fluorescence signal disappeared on the 26th day (Figure 7a and 7c). The experimental results demonstrated that our novel UV light-controlled ADC **11** had a long half-life similar to that of the monoclonal antibody Mil40. This indicated that the novel UV light-controlled ADC maintained the excellent drug-like properties of the marketed ADCs, such as excellent pharmacokinetic properties and significant tumor targeting effect *in vivo*. In addition, the fluorescence intensity in the liver was higher, while no significant fluorescence accumulation was observed in other normal tissues and organs (Figure 7b). As for the fluorescence in the liver, it was supposed to be the result that ADC **11** needed to be metabolized here. However, at the same time, it is worth noting that hepatotoxicity might be one of the main considerations in further studies. Although our design of Cys-linker-MMAE might reduce toxicity to some extent, the real safety of UV-controlled ADCs has yet to be verified by additional *in vitro* and *in vivo* experiments. After all, it was a difficult lesson that the first ADC Mylotarg was once withdrawn from the market because of serious hepatotoxicity.

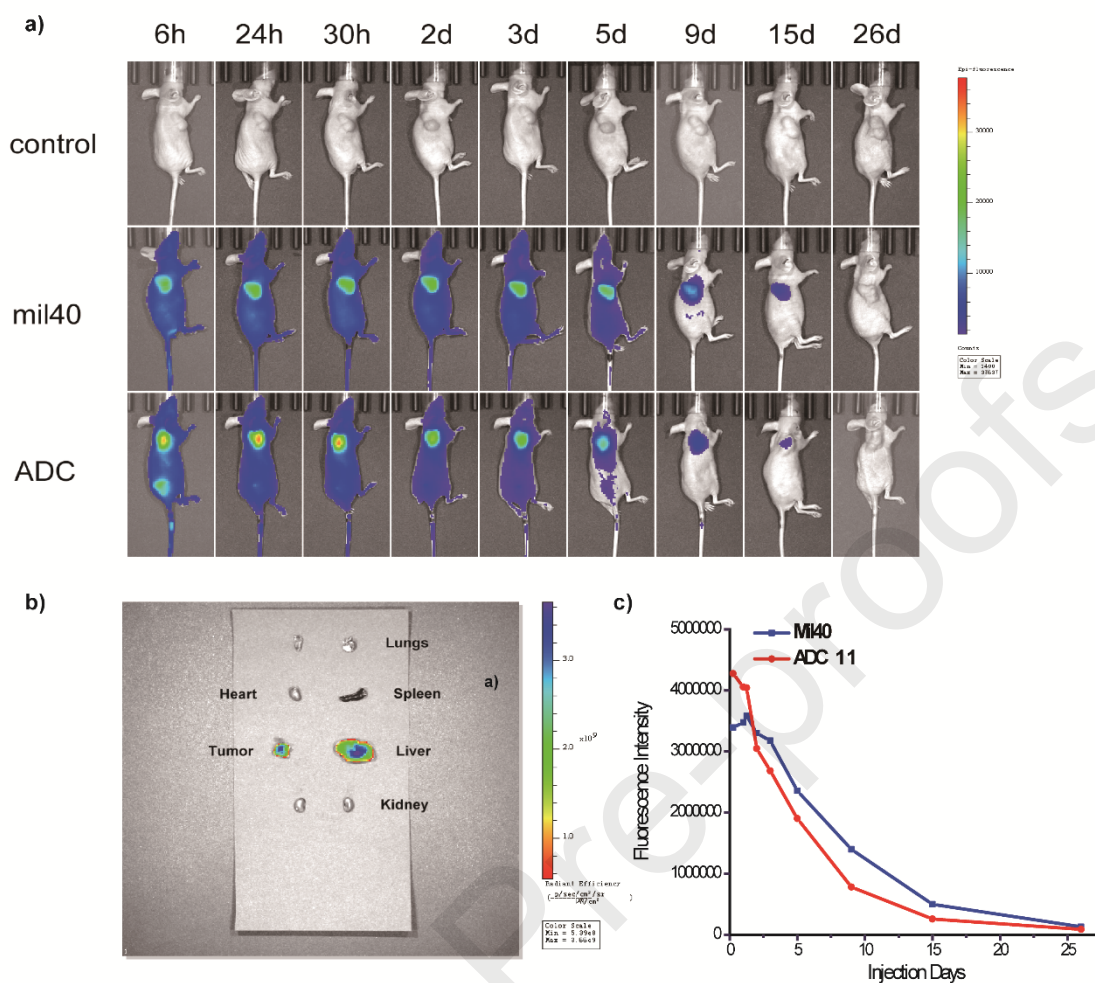


**Figure 7.** *In vivo* imaging of fluorescein-labeled ADC 11. (a) *In vivo* fluorescence imaging of DyLight 680 NHS Ester-labeled Mil40 and ADC 11 in NCI-N87 BALB/c nude mice. ADC 11 has similar tumor targeting ability and fluorescence quenching time as the Mil40. (b) Higher fluorescence accumulation in tumor as compared to other normal organs support tumor selectivity of ADC 11. (c) Quantitative analysis of fluorescent signals. ADC 11 and Mil40 have similar fluorescence in mice, and the fluorescence signal gradually decreases over time.

### 3. Materials and Methods

#### 3.1. Chemistry

Reagents and solvents were purchased from Innochem, Energy Chemical, Aladdin, Adamas-beta, TCI, Ark Pharm, Acros and Alfa Aesar and were used without additional purification. Mil40 is a biosimilar of trastuzumab, which was provided by Zhejiang Haizheng Pharmaceutical Co., Ltd. Reactions were followed by thin-layer chromatography (Dexin Biotechnology Co., Ltd, Yantai, China). Visualization was accomplished with 254 nm UV light. Nuclear magnetic resonance (NMR) spectra were obtained on a JNM-ECA-400. Chemical shifts are reported in ppm, and TMS is used as the internal standard. Coupling constants *J* are given in Hertz. Spin multiplicities are reported as the following abbreviations: s (singlet), d (doublet), dd (doublet doublet), t (triplet), q (quadruplet), and m (multiplet). Mass spectrometry (MS) was performed on a triple quadrupole mass spectrometer using electrospray ionization, API 3000 (AB Sciex, Concord, ON, Canada).

##### 3.1.1. Synthesis of ethyl 4-(4-acetyl-2-methoxyphenoxy) butanoate (**3**)

A mixture of 1-(4-hydroxy-3-methoxyphenyl)ethan-1-one (15 g, 90.27 mmol) and ethyl 4-bromobutanoate (21.13 g, 108.33 mmol) in anhydrous DMF (200 mL) and K<sub>2</sub>CO<sub>3</sub> (24.95 g, 180.52 mmol) was added.

Then, the mixture was heated to 50°C for 6 h. After the reaction was cooled to room temperature, the mixture was filtered, and the filtrate was partitioned between water (500 mL) and ethyl acetate (500 mL × 3). The combined organic layers were washed with brine, dried over anhydrous sodium sulfate, and concentrated to give a crude product. The crude product was purified by column chromatography (petroleum ether/ethyl acetate = 5:1) to give ethyl 4-(4-acetyl-2-methoxyphenoxy) butanoate (23.2 g, yield 92%) as a white solid; <sup>1</sup>H NMR (400 MHz, DMSO-d<sub>6</sub>): δ 7.60 (dd, *J* = 8.4, 2.0 Hz, 1H), 7.43 (d, *J* = 2.0 Hz, 1H), 7.05 (d, *J* = 8.4 Hz, 1H), 4.09 – 4.04 (m, 4H), 3.81 (s, 3H), 2.52 (s, 3H), 2.46 (t, *J* = 7.3 Hz, 2H), 2.02 – 1.95 (m, 2H), 1.18 (t, *J* = 7.1 Hz, 3H). ESI *m/z* (M + H)<sup>+</sup> calculated for C<sub>15</sub>H<sub>21</sub>O<sub>5</sub><sup>+</sup> 281.13; found 281.14.

### 3.1.2. Synthesis of ethyl 4-(4-acetyl-2-methoxy-5-nitrophenoxy) butanoate (**4**)

A mixture of 70% HNO<sub>3</sub> (100 mL) and acetic anhydride (20 mL) was cooled to 0°C. A suspension of **3** (5.0 g, 17.8 mmol) in acetic anhydride (15 mL) was added dropwise, and the mixture was stirred for 5 h at 0°C. After the reaction was completed, the solution was poured into ice water and cooled in the refrigerator for 2 h. The resulting solid was collected by filtration, washed with water (40 mL × 2) to remove excess acid, and dried to afford ethyl 4-(4-acetyl-2-methoxy-5-nitrophenoxy) butanoate (4.44 g, yield 77%) as a light yellow solid; <sup>1</sup>H NMR (400 MHz, DMSO-d<sub>6</sub>): δ 7.63 (s, 1H), 7.23 (s, 1H), 4.13 (t, *J* = 6.4 Hz, 2H), 4.07 (q, *J* = 7.1 Hz, 2H), 3.93 (s, 3H), 2.51 (d, *J* = 2.4 Hz, 3H), 2.46 (t, *J* = 7.3 Hz, 2H), 2.03 – 1.96 (m, 2H), 1.18 (t, *J* = 7.1 Hz, 3H). ESI *m/z* (M + H)<sup>+</sup> calculated for C<sub>15</sub>H<sub>20</sub>NO<sub>7</sub><sup>+</sup> 326.12; found 326.12.

### 3.1.3. Synthesis of 4-(4-(1-hydroxyethyl)-2-methoxy-5-nitrophenoxy) butanoic acid (**5**)

Compound **4** (4.3 g, 13.2 mmol) was added to a hot acidic solution of acetic acid (20 mL) and water (60 mL), followed by the addition of concentrated hydrochloric acid (5 mL). The mixture was stirred at reflux for 1 h. The solution was cooled to room temperature when it became completely transparent. The precipitate was filtered and collected and washed with water (200 mL × 2) to afford the crude product used directly in the next reaction. The crude product was dispersed in an aqueous solution (150 mL), and sodium hydrogencarbonate (2.45 g, 29.2 mmol) was added in batches. Ethanol (9 mL) was added dropwise to remove the foam. Then, within one hour, sodium borohydride was added, and the pH was maintained in the range of 9-11 by the addition of sodium bicarbonate. After 2 h, the reaction was acidified to pH=2 with 8 N HCl. The mixture was filtered, washed with water (200 mL × 2), and dried to afford 4-(4-(1-hydroxyethyl)-2-methoxy-5-nitrophenoxy) butanoic acid (3.21 g, yield 81%) as a yellow solid; <sup>1</sup>H NMR (400 MHz, DMSO-d<sub>6</sub>): δ 12.19 (s, 1H), 7.53 (s, 1H), 7.35 (s, 1H), 5.49 (d, *J* = 4.4 Hz, 1H), 5.28 – 5.22 (m, 1H), 4.05 (t, *J* = 6.5 Hz, 2H), 3.90 (s, 3H), 2.38 (t, *J* = 7.3 Hz, 2H), 1.98 – 1.91 (m, 2H), 1.36 (d, *J* = 6.2 Hz, 3H). ESI *m/z* (M - H)<sup>-</sup> calculated for C<sub>13</sub>H<sub>16</sub>NO<sub>7</sub><sup>-</sup> 298.09; found 298.10.

### 3.1.4. Synthesis of tert-butyl (2-(4-(4-(1-hydroxyethyl)-2-methoxy-5-nitrophenoxy)butanamide-do) ethyl) carbamate (**6**)

To a solution of **5** (1.7 g, 5.68 mmol) in anhydrous DMF (30 mL), HOBt (920 mg, 6.82 mmol), EDCI (1.63 g, 8.53 mmol), and DIPEA (1.1 g, 8.53 mmol) were added sequentially to the reaction solution. Then, tert-butyl (2-aminoethyl) carbamate (1.09 g, 6.82 mmol) was added, and the mixture was stirred at room temperature overnight. After the reaction was completed, the mixture was treated with water (100 mL) and extracted with ethyl acetate (50 mL × 3). The combined organic layers were washed with brine, dried over anhydrous sodium sulfate, and concentrated to give a crude product, which was purified by column chromatography (ethyl acetate) to give tert-butyl (2-(4-(4-(1-hydroxyethyl)-2-methoxy-5-nitrophenoxy)butanamide-do) ethyl) carbamate (1.54 g, yield 61%) as a light yellow solid; <sup>1</sup>H NMR (400 MHz, DMSO-d<sub>6</sub>) δ 7.88 (t, *J* = 5.4 Hz, 1H), 7.52 (s, 1H), 7.35 (s, 1H), 6.80 (t, *J* = 5.5 Hz, 1H), 5.49 (d, *J* = 4.4 Hz, 1H), 5.28 – 5.22 (m, 1H), 4.03 (t, *J* = 6.4 Hz, 2H), 3.90 (s, 3H), 3.06 (dd, *J* = 12.1, 5.9 Hz, 2H), 2.96 (dd, *J* = 12.1, 6.0 Hz, 2H), 2.22 (t, *J* = 7.4 Hz, 2H), 1.97 – 1.91 (m, 2H), 1.36 (t, *J* = 2.9 Hz, 12H). ESI *m/z* (M + H)<sup>+</sup> calculated for C<sub>20</sub>H<sub>32</sub>N<sub>3</sub>O<sub>8</sub><sup>+</sup> 442.22; found 442.21.

### 3.1.5. Synthesis of *N*-(2-aminoethyl)-4-(4-(1-hydroxyethyl)-2-methoxy-5-nitrophenoxy) butan-amide (**7**)

To a suspension of **6** (1.5 g, 3.4 mmol) in methanol (20 mL) was added a solution of HCl (6 N, 20 mL). The reaction mixture was stirred at room temperature for 5 h, concentrated, and dried under vacuum to afford a crude product of N-(2-aminoethyl)-4-(4-(1-hydroxyethyl)-2-methoxy-5-nitrophenoxy)-butanamide as a yellow liquid, which was used directly in the next reaction.

### 3.1.6. Synthesis of 6-(2,5-dioxo-2,5-dihydro-1H-pyrrol-1-yl)-N-(2-(4-(4-(1-hydroxyethyl)-2-methoxy-5-nitrophenoxy)butanamido)ethyl) hexanamide (**9a**)

To a suspension of **7** (700 mg, 2.05 mmol) in anhydrous DMF (20 mL) was added compound **8a** (694.8 mg, 2.26 mmol). DIPEA (317.9 mg, 2.46 mmol) was added to the reaction solution, and then the mixture was stirred at room temperature overnight and evaporated under reduced pressure to give the crude product. The crude product was purified by column chromatography (dichloromethane/methanol = 50:1 to 10:1) to give **9a** (955 mg, yield 87%) as a light yellow solid; <sup>1</sup>H NMR (400 MHz, DMSO-d<sub>6</sub>): δ 7.89 (s, 1H), 7.80 (s, 1H), 7.52 (s, 1H), 7.35 (s, 1H), 7.00 (s, 2H), 5.49 (d, *J* = 4.4 Hz, 1H), 5.28 – 5.22 (m, 1H), 4.02 (t, *J* = 6.4 Hz, 2H), 3.90 (s, 3H), 3.37 (d, *J* = 7.1 Hz, 2H), 3.07 – 3.06 (m, 4H), 2.22 (t, *J* = 7.4 Hz, 2H), 2.00 (t, *J* = 7.4 Hz, 2H), 1.96 – 1.91 (m, 2H), 1.49 – 1.42 (m, 4H), 1.36 (d, *J* = 6.2 Hz, 3H), 1.19 – 1.12 (m, 2H). ESI *m/z* (*M* + *H*)<sup>+</sup> calculated for C<sub>25</sub>H<sub>35</sub>N<sub>4</sub>O<sub>9</sub><sup>+</sup> 535.24; found 535.22.

### 3.1.7. Synthesis of N-(16-(2,5-dioxo-2,5-dihydro-1H-pyrrol-1-yl)-4,14-dioxo-7,10-dioxa-3,13-diazahexadecyl)-4-(4-(1-hydroxyethyl)-2-methoxy-5-nitrophenoxy) butanamide (**9b**)

Compound **9b** was synthesized by employing the experimental protocols described for **9a**. The yield was 51% as a light yellow solid. <sup>1</sup>H NMR (400 MHz, DMSO-d<sub>6</sub>) δ 8.04 (t, *J* = 5.6 Hz, 1H), 7.90 (s, 2H), 7.52 (s, 1H), 7.35 (s, 1H), 7.00 (s, 2H), 5.49 (d, *J* = 4.4 Hz, 1H), 5.28 – 5.22 (m, 1H), 4.03 (t, *J* = 6.4 Hz, 2H), 3.90 (s, 3H), 3.60 – 3.56 (m, 4H), 3.46 (d, *J* = 2.8 Hz, 4H), 3.40 – 3.37 (m, 2H), 3.15 – 3.11 (m, 2H), 3.08 – 3.07 (m, 4H), 2.34 – 2.27 (m, 4H), 2.25 – 2.21 (m, 2H), 1.98 – 1.93 (m, 2H), 1.36 (d, *J* = 6.2 Hz, 3H). ESI *m/z* (*M* + *H*)<sup>+</sup> calculated for C<sub>29</sub>H<sub>42</sub>N<sub>5</sub>O<sub>12</sub><sup>+</sup> 652.28; found 652.29.

### 3.1.8. Synthesis of 1-(4-(4-((2-(6-(2,5-dioxo-2,5-dihydro-1H-pyrrol-1-yl)hexanamido)ethyl)-amino)-4-oxobutoxy)-5-methoxy-2-nitrophenyl)ethyl (4-nitrophenyl) carbonate (**10a**)

Bis(4-nitrophenyl) carbonate (1.08 g, 3.56 mmol) was added to a suspension of compound **9a** (950 mg, 1.78 mmol) and DIPEA (690 mg, 5.34 mmol) in anhydrous DMF (20 mL). Then, the mixture was stirred at room temperature overnight and evaporated under reduced pressure to give the crude product, which was purified by column chromatography (dichloromethane/methanol = 50:1 to 10:1) to give **10a** (522.5 mg, yield 42%) as a light yellow solid; <sup>1</sup>H NMR (400 MHz, DMSO-d<sub>6</sub>) δ 8.31 – 8.27 (m, 2H), 7.90 (s, 1H), 7.80 (s, 1H), 7.59 (s, 1H), 7.55 – 7.51 (m, 2H), 7.18 (s, 1H), 7.00 (s, 2H), 6.27 (q, *J* = 6.5 Hz, 1H), 4.06 (t, *J* = 6.4 Hz, 2H), 3.96 (s, 3H), 3.36 (d, *J* = 7.1 Hz, 2H), 3.07 – 3.06 (m, 4H), 2.23 (t, *J* = 7.4 Hz, 2H), 2.00 (t, *J* = 7.3 Hz, 2H), 1.97 – 1.92 (m, 2H), 1.72 (d, *J* = 6.5 Hz, 3H), 1.49 – 1.41 (m, 4H), 1.19 – 1.11 (m, 2H). ESI *m/z* (*M* + *H*)<sup>+</sup> calculated for C<sub>32</sub>H<sub>38</sub>N<sub>5</sub>O<sub>13</sub><sup>+</sup> 700.24; found 700.25.

### 3.1.9. Synthesis of 1-(4-((1-(2,5-dioxo-2,5-dihydro-1H-pyrrol-1-yl)-3,13,18-trioxo-7,10-dioxa-4,14,17-triazahenicosan-21-yl)oxy)-5-methoxy-2-nitrophenyl)ethyl (4-nitrophenyl) carbonate (**10b**)

Compound **10b** was synthesized by employing the experimental protocols described for **10a**. The yield was 44% as a light yellow solid; <sup>1</sup>H NMR (400 MHz, DMSO-d<sub>6</sub>) δ 8.29 (d, *J* = 9.1 Hz, 2H), 8.04 (t, *J* = 5.6 Hz, 1H), 7.90 (s, 2H), 7.59 (s, 1H), 7.53 (d, *J* = 9.0 Hz, 2H), 7.19 (s, 1H), 7.00 (s, 2H), 6.27 (dd, *J* = 12.7, 6.1 Hz, 1H), 4.07 (t, *J* = 6.3 Hz, 2H), 3.96 (s, 3H), 3.60 – 3.56 (m, 4H), 3.49 (d, *J* = 5.0 Hz, 2H), 3.36 – 3.33 (m, 4H), 3.13 (dd, *J* = 11.3, 5.7 Hz, 2H), 3.08 (s, 4H), 2.34 – 2.27 (m, 4H), 2.23 (t, *J* = 7.5 Hz, 2H), 1.99 – 1.94 (m, 2H), 1.72 (d, *J* = 6.4 Hz, 3H). ESI *m/z* (*M* + *H*)<sup>+</sup> calculated for C<sub>38</sub>H<sub>45</sub>N<sub>6</sub>O<sub>16</sub><sup>+</sup> 817.28; found 817.29.

### 3.1.10. Synthesis of compound **1a**

To a solution of **10a** (85.76 mg, 0.12 mmol) in anhydrous DMF (15 mL), HOBT (15.06 mg, 0.11 mmol), DIPEA (28.43 mg, 0.22 mmol), and MMAE (80 mg, 0.11 mmol) were added sequentially, and then the mixture

was stirred at room temperature for 12 h. After the reaction was completed, the mixture was evaporated under reduced pressure to give the crude product, which was purified by column chromatography (dichloromethane/methanol = 70:1 to 15:1) to give **1a** (87 mg, yield 62%) as a yellow solid; <sup>1</sup>H NMR (400 MHz, DMSO-*d*<sub>6</sub>) δ 7.87 (d, *J* = 12.9 Hz, 2H), 7.76 (s, 1H), 7.61 (d, *J* = 8.4 Hz, 1H), 7.52 – 7.44 (m, 2H), 7.26 – 7.21 (m, 4H), 7.14 (t, *J* = 7.0 Hz, 1H), 6.96 (s, 2H), 6.11 – 6.06 (m, 1H), 5.39 (d, *J* = 4.6 Hz, 1H), 5.32 (d, *J* = 4.7 Hz, 1H), 4.77 – 4.48 (m, 2H), 4.47 – 4.31 (m, 2H), 4.04 – 3.81 (m, 8H), 3.54 – 3.43 (m, 2H), 3.37 – 3.32 (m, 2H), 3.24 – 3.17 (m, 5H), 3.15 – 3.08 (m, 4H), 3.02 (s, 5H), 2.98 – 2.89 (m, 3H), 2.73 (t, *J* = 17.3 Hz, 2H), 2.19 (t, *J* = 6.5 Hz, 3H), 2.08 (s, 2H), 1.97 (t, *J* = 7.4 Hz, 3H), 1.91 (s, 3H), 1.80 – 1.61 (m, 4H), 1.58 – 1.52 (m, 3H), 1.46 – 1.37 (m, 5H), 1.16 – 1.09 (m, 2H), 1.02 – 0.92 (m, 6H), 0.87 – 0.67 (m, 17H). ESI *m/z* (*M* + *H*)<sup>+</sup> calculated for C<sub>65</sub>H<sub>100</sub>N<sub>9</sub>O<sub>17</sub><sup>+</sup> 1278.7232; found 1278.7231.

### 3.1.11. Synthesis of compound **1b**

Compound **1b** was synthesized by employing the experimental protocols described for **1a**. The yield was 66% as a light yellow solid; <sup>1</sup>H NMR (400 MHz, DMSO-*d*<sub>6</sub>) δ 8.03 (s, 1H), 7.91 (d, *J* = 12.3 Hz, 3H), 7.65 (d, *J* = 8.1 Hz, 1H), 7.61 – 7.47 (m, 2H), 7.32 – 7.25 (m, 4H), 7.17 (t, *J* = 6.7 Hz, 1H), 7.00 (s, 2H), 6.20 – 6.08 (m, 1H), 5.44 (s, 1H), 5.36 (s, 1H), 4.81 – 4.58 (m, 2H), 4.50 – 4.36 (m, 2H), 4.07 – 3.84 (m, 8H), 3.63 – 3.52 (m, 6H), 3.46 (s, 5H), 3.26 – 3.20 (m, 5H), 3.19 – 3.12 (m, 6H), 3.08 (s, 5H), 3.02 – 2.93 (m, 3H), 2.76 (t, *J* = 17.1 Hz, 2H), 2.36 – 2.25 (m, 5H), 2.22 (s, 2H), 2.16 – 1.89 (m, 6H), 1.78 (s, 4H), 1.64 – 1.43 (m, 5H), 1.06 – 0.96 (m, 6H), 0.93 – 0.71 (m, 17H). ESI *m/z* (*M* + *H*)<sup>+</sup> calculated for C<sub>69</sub>H<sub>107</sub>N<sub>10</sub>O<sub>20</sub><sup>+</sup> 1395.7658; found 1395.7637.

## 3.2. Bioconjugation and Purification

Antibody-conjugated drugs **11** and **12** were synthesized according to the following method.

### 3.2.1. Antibody reduction

Humanized anti-HER2 IgG1 antibody mil40 (5 mg/mL) was dissolved in pH 7.5, 20 mM L-histidine buffer. Reductant tris(2-carboxyethyl) phosphine hydrochloride (TECP; 2.3 equivalents) was added, and then the mixture was stirred at 25°C for 2 h.

### 3.2.2. Antibody conjugation

To a solution of reduced mil40 was added maleimide-containing compound **1a** or **1b** (8 equivalents) in ice-cold dimethylacetamide (DMAC) (5% v/v). The mixture was stirred at 25°C for 50 min.

### 3.2.3. Termination reaction

The reaction solution was added excess N-acetyl-L-cysteine (10 equivalents) to quench. After stirring for 30 min, the mixture was acidified to pH=5.5 with 0.3M AcOH.

### 3.2.4. Purification and analysis

The mixture was allowed to be buffer exchanged using AKTA pure 25 (GE Healthcare, USA) and Sephadex G-25 Medium buffer exchange columns to afford conjugates **11** or **12**. The conjugates were concentrated by ultrafiltration centrifugation and sterile filtered through a 0.2 μm filter under sterile conditions. Then, the samples were stored at -80°C before use for analysis and testing. The drug-to-antibody ratio (DAR) was determined by using HIC HPLC (Agilent 1260 HPLC; Wilmington, DE, USA); a UV-visible spectrophotometer (UV-2450, SHIMADZU, Japan) was used to determine the concentration of conjugates.

## 3.3. Linker-MMAE Stability Assays In Vitro

ADCs **11** and **12** (100 nM) were incubated with 50% human plasma. The reaction mixture was incubated at 37 °C in a constant temperature incubator. After 48, 96, 120, and 144 h, aliquot samples (50 μL) were taken,

and methanol (250  $\mu$ L) was added to the samples. The solution was centrifuged, and the released MMAE was analyzed by LC-MS.

Compounds **1a** and **1b** were dissolved in DMSO (1 mg/ml), followed by the addition of L-cysteine PBS solution (0.095 mg/ml, pH 7.4). The final DMSO concentration was controlled at 10%, and the mixture was stirred at room temperature for 10 min, after which HPLC analysis revealed complete conversion to Cys-**1a** and Cys-**1b**. The reaction mixture was incubated at 37 °C in a constant temperature incubator. After 0, 5, 10, 15, and 30 min and 1, 2, 4, 8, 12, 24, 48, 72, and 168 h, aliquot samples (300  $\mu$ L) were taken and frozen at -20 °C. All samples were melted in sequence, and analysis was performed by HPLC.

#### 3.4. UV-cleavage tests on the linker-MMAE *In Vitro*

Compounds were dissolved in methyl alcohol (40  $\mu$ M), and the solutions were irradiated at 365 nm by using an ultraviolet crosslinker (CL-1000 L UVP Crosslinker, 5 $\times$ 8 W, Analytikjena, USA). Every minute from 0 to 10 min, aliquot samples (400  $\mu$ L) were taken and analyzed by HPLC.

#### 3.5. ADC Affinity Assay

The HER2 affinity of ADC was measured by ELISA. In brief, HER2 antigen (Her2 protein, Human, Recombinant, Sino Biological Inc., Beijing, China) was diluted to a final concentration of 1  $\mu$ g/mL with coating solution and plated on 96-well plates (100  $\mu$ L for each well) at 4 °C overnight in a wet box. The coating solution was removed, and the remaining protein-binding sites were blocked by incubation with 10% fetal bovine serum for 2 h at 37°C. Reactions were initiated by adding gradient concentrations of ADC. After reacting for 1 h, the plate was washed with PBS (containing 0.2% Tween) three times. Then, 100  $\mu$ L of goat anti-human IgG Fc cross-absorbed secondary antibody conjugated to HRP (Thermo Fisher Scientific, USA) was added to each well and incubated for 45 min at room temperature. Then, the plate was washed three times with PBS (containing 0.2% Tween). TMB was added to develop color (100  $\mu$ L for each well) and protected from light for 1 min. Finally, 2 M H<sub>2</sub>SO<sub>4</sub> was used to stop the reaction, and the absorbance of each well was read at 450 nm with a multifunction microplate reader.

#### 3.6. Flow Cytometry Assay

MCF-7 and BT474 cells obtained from ATCC (Manassas, VA, USA) were resuspended in 200  $\mu$ L PBS (pH 7.4, containing 2% fetal bovine serum) and incubated with 5  $\mu$ g/ml mil40 or ADC at a density of 5  $\times$  10<sup>5</sup> cells/ml for 30 min at 4°C. After being washed twice with PBS, the cells were further incubated with 10  $\mu$ g/ml PE-labeled anti-human IgG Fc (BioLegend, USA) for 30 min at 4°C. Then, the cells were washed twice with PBS. The fluorescence intensity of PE was measured using a NovoCyte flow cytometer (ACEA Bioscience, Hangzhou, China). Data were analyzed by using FlowJo software. For BT474-HerDR cells and N87-HerDR cells provided by Yicon (Beijing) Medical Science And Technology Co., Ltd., fluorescence intensity measurements can be performed only after incubation with FITC anti-human HER2 antibody (BioLegend, USA). FITC mouse IgG was used as an isotype control (BioLegend, USA).

#### 3.7. Fluorescence microscopy

BT474 cells (5 $\times$ 10<sup>4</sup>/dish) were plated in new confocal dishes, cultured in RPMI-1640 medium with 10% fetal bovine serum at 37°C and 5% CO<sub>2</sub>, and then incubated with 1 ml (10  $\mu$ g/ml) ADC or positive control antibody mil40 for 30 min on ice or 24 h at 37°C. Lysosomal protease inhibitors (25 nM) were added to all the dishes. The cells were washed with prechilled PBS, fixed and permeabilized with 0.5% BSA and 0.5% Triton X-100 PBS solution at 37°C for 5 min. After washing with prechilled PBS, ADC or mil40, the lysosomal compartment was detected using 3  $\mu$ g/mL Alexa Fluor 488-labeled goat anti-human IgG (BioLegend, USA) and 3  $\mu$ g/mL Alexa Fluor 647-labeled anti-human CD107b antibody (Invitrogen, Carlsbad, California, USA), respectively. Next, the nuclear compartment was stained with 10  $\mu$ g/ml DAPI at 4°C for 30 min. The cells were washed three times with prechilled PBS, and fluorescence images were taken using a confocal microscope (Leica, TCS SP8).

#### 3.8. Cell Proliferation Assay

To assess the cytotoxicity of test compounds on 3 cell lines in the presence or absence of ultraviolet radiation, cells were seeded in 96-well plates (2500 per well) and allowed to adhere overnight at 37°C in a humidified atmosphere of 5% CO<sub>2</sub>. The medium was then removed from the plates, and the cells were treated in their recommended growth media containing varying concentrations of test compounds. When the cells were incubated with the drug for 2 h, the cell culture plates were taken and irradiated to the corresponding time with an ultraviolet crosslinker (this step is only for compounds that required UV irradiation). After 96 hours of incubation, CellTiter 96® Aqueous One Solution (Promega, Madison, Wisconsin, USA) was added to the plates and incubated for 3 hours at 37°C. EC<sub>50</sub> values were calculated using GraphPad Prism 5.0.

### 3.9. Tubulin Polymerization Inhibition Assay

A tubulin polymerization assay kit (BK011P, Cytoskeleton, USA) was used to detect tubulin polymerization. All experimental steps followed the operating manual. First, 5 µL of inhibitors at various concentrations were incubated in 96-well plates at 37°C for 1 min. Then, 50 µL of the tubulin reaction solution containing 10 mg/ml porcine brain tubulin (>99% pure), 0.5 mM EGTA, 2 mM MgCl<sub>2</sub>, 60% glycerol and 100 mM GTP was added. The increase in fluorescence was measured immediately by excitation at 360 nm and emission at 420 nm in a multimode plate reader (PerkinElmer, USA).

### 3.10. *In vivo* fluorescence imaging experiment

*In vivo* fluorescence imaging experiments were implemented using the NCI-N87 BALB/c nude mouse xenograft model. Mil40 and ADC **11** were labeled with DyLight 680 NHS ester according to the manufacturer's operating manual (DyLight Amine-Reactive Dyes, Thermo Fisher Scientific). NCI-N87 cells were injected in the right dorsum of the mice subcutaneously. When the tumor volumes reached approximately 300-400 mm<sup>3</sup>, fluorescently labeled compounds were injected via the tail veins at a dose of 20 mg/mg in each mouse. Isoflurane-anesthetized mice were placed in the optical imaging chamber of an IVIS SPECTRUM mouse live imager (PerkinElmer, USA) at corresponding time points for *in vivo* distribution observation. Tumors and organs were dissected 30 hours after the injection to observe organ uptake. The images were analyzed by Living Image software.

## 4. Discussion

Although several admirable works considering photocontrolled ADCs using near infrared light (650 - 900 nm) have been reported, we developed novel UV-light (360 nm) control ADCs for the following points. First, compared with the complex structure of near infrared light-controlled ADCs, UV light-controlled ADCs have a more reasonable and simple structure and retain the structure of the marketed ADCs. Only a minor structural modification has been made by replacing PAB with the commonly used PPG group *o*-nitrobenzyl. Therefore, from the point of chemistry and pharmacology, our novel ADCs could maintain the excellent drug-like properties of the marketed ADCs, such as good plasma stability ( $t_{1/2} > 6$  days), long half-life *in vivo* (nearly the same as that of Mil40) and significant tumor targeting effect *in vivo*. In addition, research on the toxicity and membrane permeability of Cys-**1a/1b** suggested that the off-target toxicity might be lower for our ADCs. Off-target toxicity was one of the main obstacles to the development of ADC, and the first ADC Mylotarg was withdrawn once from the market because of serious off-target toxicity. However, we also admit that more *in vitro* and *in vivo* experiments are needed to verify our assumption. The Cys-linker-MMAE degradation product was detected in cells in our recent study<sup>36</sup>.

Second, concerning the clinical application of UV light-controlled ADCs, we must admit that there are still some difficulties at present. Although UVA irradiation (wavelengths above 320 nm) causes less direct DNA damage than UVB or UVC exposure, a high dosage of UVA is toxic and can lead to oxidative stress, photoaging and immunosuppression<sup>37, 38</sup>. Moreover, UV blue light cannot penetrate patient skin to reach deeply into the tumor area<sup>37, 38</sup>. Only depths of approximately 100 µm can be reached<sup>37, 38</sup>. There are several possible solutions in future clinical applications: the required light could be transmitted to the site of interest via optical fibers or endoscopic probes. Moreover, in selected cases, adjacent areas could be illuminated during the surgery<sup>25</sup>. At the same time, it should be noted that some works have been done on the application of UV-light-based therapy. For instance, psoralen plus UV-A (PUVA) therapy has been applied in dermatology since the 1970s<sup>39</sup>. Moreover, UV-light controlled small molecule prodrugs are also continuously developed, such as

photoactivatable prodrugs of the antimelanoma agent vemurafenib<sup>25</sup> and photoactivatable caged prodrugs of VEGFR-2 kinase inhibitors<sup>40</sup>. We think that these novel UV light-controlled ADCs are a good complement to the application of UV light for medical/therapeutic purposes.

## 5. Conclusions

This article reports, for the first time, the use of UV light to control drug release by ADCs. The feasibility of such a design was also preliminarily validated. Throughout the study, our ADCs exhibited good stability and photocontrollability while maintaining a targeting effect similar to that of a naked antibody. Brief UV light irradiation resulted in rapid release of small-molecule cytotoxins and effective killing of Herceptin-resistant N87-HerDR and BT474-HerDR cells. Compared with those of unirradiated ADCs, the inhibitory activities of irradiated ADCs increased by 15- and 50-fold in N87-HerDR and BT474-HerDR cells, respectively. Furthermore, the degradation product of unirradiated ADCs, Cys-1a, exhibited lower toxicity and had the potential to reduce the toxic adverse effects caused by nonspecific uptake of ADCs. The potential applications of this novel type of UV light-controlled ADC include the use of fiber optic or endoscopic probes to transmit the required light to the site of action or by irradiating the lesion during surgery. ADCs can also be used as cell tool drugs. However, there are some limitations in this study that require further investigation. The first is the optimization of the linker structure. Compound 1a can serve as a good lead compound, and its structure can be modified to further reduce its toxicity. Second, the binding of ADCs and cells was only studied under ideal conditions at 2 h, which was useful to elucidate the basic properties of UV-controlled ADCs. However, the situation after ADCs enter the cells is more complex, and more work is needed in the future to thoroughly understand this process. Overall, the novel design strategy for ADCs proposed in this study provides a new tool for future mechanistic research on ADCs and new perspectives on the development of novel types of ADCs for therapeutic applications.

**Author Contributions:** conceptualization, D.X.; methodology, J.L.; software, L.Z.; validation, W.S., X.Y. and X.Z.; formal analysis, J.L. and F.X.; investigation, D.X. and W.L.; resources, X.Z.; data curation, J.L. and W.L.; writing—original draft preparation, J.L.; writing—review and editing, W.S., X.Y. and X.Z.; supervision, X.Y. and X.Z.; project administration, X.Z.; funding acquisition, X.Z.”

**Funding:** This research was funded by the National Science and Technology Major Project for Major New Drugs Innovation and Development under grant no. 2018ZX09711003-009 and Chinese National Natural Science Foundation under grant no. 81872736.

**Acknowledgments:** The authors gratefully acknowledge research support from Dan Jiang laboratory for the structural confirmation.

**Conflicts of Interest:** The authors declare no conflict of interest.

## References

1. Beck, A.; Haeuw, J. F.; Wurch, T.; Goetsch, L.; Bailly, C.; Corvaia, N., The next generation of antibody-drug conjugates comes of age. *Discovery Medicine* **2010**, *10* (53), 329-39.
2. Leal, M.; Sapra, P.; Hurvitz, S. A.; Senter, P.; Wahl, A.; Schutten, M.; Shah, D. K.; Haddish-Berhane, N.; Kabbarah, O., Antibody-drug conjugates: an emerging modality for the treatment of cancer. *Annals of the New York Academy of Sciences* **2015**, *1321* (1), 41-54.
3. Sievers, E. L.; Senter, P. D., Antibody-Drug Conjugates in Cancer Therapy. *Annual Review of Medicine* **2013**, *64* (3), 15-29.
4. Lyon, R., Drawing lessons from the clinical development of antibody-drug conjugates. *Drug Discovery Today: Technologies* **2018**, *30*, 105-109.
5. Coats, S.; Williams, M.; Keble, B.; Dixit, R.; Tseng, L.; Yao, N. S.; Tice, D. A.; Soria, J. C., Antibody-Drug Conjugates: Future Directions in Clinical and Translational Strategies to Improve the Therapeutic Index. *Clinical cancer research : an official journal of the American Association for Cancer Research* **2019**.
6. Jain, N.; Smith, S.; Ghone, S.; Tomczuk, B., Current ADC Linker Chemistry. *Pharm Res* **2015**, *32* (11), 3526-3540.
7. Lu, J.; Feng, J.; Aiping, L.; Ge, Z., Linkers Having a Crucial Role in Antibody-Drug Conjugates. *International Journal of Molecular Sciences* **2016**, *17* (4), 561-.

8. Tsuchikama, K.; An, Z., Antibody-drug conjugates: recent advances in conjugation and linker chemistries. *Protein & Cell* **2018**, *9* (1), 33-46.
9. Sorokin, P., Mylotarg approved for patients with CD33+ acute myeloid leukemia. *Clinical journal of oncology nursing* **2000**, *4* (6), 279-80.
10. Ricart; D., A., Antibody-Drug Conjugates of Calicheamicin Derivative: Gemtuzumab Ozogamicin and Inotuzumab Ozogamicin. *Clinical Cancer Research* **2011**, *17* (20), 6417-6427.
11. Deng, C.; Pan, B.; O'Connor, O. A., Brentuximab vedotin. *Clinical Cancer Research An Official Journal of the American Association for Cancer Research* **2013**.
12. Fitzgerald, D. J.; Wayne, A. S.; Kreitman, R. J.; Pastan, I., Treatment of hematologic malignancies with immunotoxins and antibody-drug conjugates. *Cancer Research* **2011**, *71* (20), 6300-6309.
13. None, Photolabile protecting groups and linkers. *Journal of the Chemical Society Perkin Transactions* **2002**, *2* (2), 125-142.
14. Fodor, S.; Read, J.; Pirrung, M.; Stryer, L.; Lu, A.; Solas, D., Light-directed, spatially addressable parallel chemical synthesis. *Science* **1991**, *251* (4995), 767-773.
15. Mcgall, G. H.; Barone, A. D.; Diggelmann, M.; Fodor, S. P. A.; Gentalen, E.; Ngo, N., The Efficiency of Light-Directed Synthesis of DNA Arrays on Glass Substrates. *Journal of the American Chemical Society* **1997**, *119* (22), 5081-5090.
16. Guillier, F.; Orain, D.; Bradley, M., Linkers and cleavage strategies in solid-phase organic synthesis and combinatorial chemistry. (Chem. Rev. 2000, 100, 2091. Published on the web may 6, 2000). *Chemical Reviews* **2000**, *100* (6), 2091.
17. Pelliccioli, A. P.; Wirz, J., Photoremovable protecting groups: reaction mechanisms and applications. *Photochemical & Photobiological Sciences Official Journal of the European Photochemistry Association & the European Society for Photobiology* **2002**, *1* (7), 441-458.
18. Rogerr., N.; Alexander P., G.; Tadanobu, N.; Tsuyoshi, Y.; Joseph, I.; Hisataka, K.; Martin J., S., In Vivo Activation of Duocarmycin-AntibodyConjugates by Near-Infrared Light. *Acs Central Science* **2017**, *3* (4), 329.
19. Nani, R. R.; Gorke, A. P.; Nagaya, T.; Kobayashi, H.; Schnermann, M. J., Near-IR Light-Mediated Cleavage of Antibody-Drug Conjugates Using Cyanine Photocages. *Angewandte Chemie International Edition* **2015**, *127* (46), 13635.
20. Xu, Y.; Li, Z.; Malkovskiy, A.; Sun, S.; Pang, Y., Aggregation Control of Squaraines and Their Use as Near-Infrared Fluorescent Sensors for Protein. *Journal of Physical Chemistry B* **2010**, *114* (25), 8574-8580.
21. Mcrae, E. G.; Kasha, M., Enhancement of Phosphorescence Ability upon Aggregation of Dye Molecules. *Journal of Chemical Physics* **1958**, *28* (4), 721-722.
22. Kaplan, J. H.; Forbush, B.; Hoffman, J. F., Rapid photolytic release of adenosine 5'-triphosphate from a protected analog: utilization by the sodium:potassium pump of human red blood cell ghosts. *Biochemistry* **1978**, *17* (10), 1929-1935.
23. Engels, J.; Schlaeger, E. J., Synthesis, structure, and reactivity of adenosine cyclic 3',5'-phosphate benzyl triesters. *Journal of Medicinal Chemistry* **1977**, *20* (7), 907-911.
24. Pinchuk, B.; Horbert, R.; Döbber, A.; Kuhl, L.; Peifer, C., Photoactivatable Caged Prodrugs of VEGFR-2 Kinase Inhibitors. *Molecules* **2016**, *21* (5), 570.
25. Horbert, R.; Pinchuk, B.; Davies, P.; Alessi, D.; Peifer, C., Photoactivatable Prodrugs of Antimelanoma Agent Vemurafenib. *Acs Chem Biol* **2015**, *10* (9), 2099-107.

26. Shin, W. S.; Han, J.; Kumar, R.; Lee, G. G.; Sessler, J. L.; Kim, J.-H.; Kim, J. S., Programmed activation of cancer cell apoptosis: A tumor-targeted phototherapeutic topoisomerase I inhibitor. *Scientific Reports* **2016**, *6*, 29018.
27. Ibsen, S.; Zahavy, E.; Wrasdilo, W.; Berns, M.; Chan, M.; Esener, S., A Novel Doxorubicin Prodrug with Controllable Photolysis Activation for Cancer Chemotherapy. *Pharmaceutical Research* **2010**, *27* (9), 1848-1860.
28. Li, H.; Yu, C.; Jiang, J.; Huang, C.; Yao, X.; Xu, Q.; Yu, F.; Lou, L.; Fang, J., An anti-HER2 antibody conjugated with monomethyl auristatin E is highly effective in HER2-positive human gastric cancer. *Cancer Biology & Therapy* **2016**, *17* (4), 346-354.
29. Jiang, J.; Dong, L.; Wang, L.; Wang, L.; Zhang, J.; Chen, F.; Zhang, X.; Huang, M.; Li, S.; Ma, W., HER2-targeted antibody drug conjugates for ovarian cancer therapy. *European Journal of Pharmaceutical Sciences* **2016**, *93*, 274-286.
30. Yao, X.; Jiang, J.; Wang, X.; Huang, C.; Li, D.; Xie, K.; Xu, Q.; Li, H.; Li, Z.; Lou, L., A novel humanized anti-HER2 antibody conjugated with MMAE exerts potent anti-tumor activity. *Breast Cancer Research & Treatment* **2015**, *153* (1), 123-133.
31. Erickson, K., H., Antibody-Maytansinoid Conjugates Are Activated in Targeted Cancer Cells by Lysosomal Degradation and Linker-Dependent Intracellular Processing. *Cancer Research* **2006**, *66* (8), 4426-4433.
32. Lewis Phillips, G. D.; Li, G.; Dugger, D. L.; Crocker, L. M.; Parsons, K. L.; Mai, E.; Blattler, W. A.; Lambert, J. M.; Chari, R. V.; Lutz, R. J.; Wong, W. L.; Jacobson, F. S.; Koeppen, H.; Schwall, R. H.; Kenkare-Mitra, S. R.; Spencer, S. D.; Sliwkowski, M. X., Targeting HER2-positive breast cancer with trastuzumab-DM1, an antibody-cytotoxic drug conjugate. *Cancer Res* **2008**, *68* (22), 9280-90.
33. Doronina, S. O.; Toki, B. E.; Torgov, M. Y.; Mendelsohn, B. A.; Cerveny, C. G.; Chace, D. F.; DeBlanc, R. L.; Gearing, R. P.; Bovee, T. D.; Siegall, C. B.; Francisco, J. A.; Wahl, A. F.; Meyer, D. L.; Senter, P. D., Development of potent monoclonal antibody auristatin conjugates for cancer therapy. *Nature biotechnology* **2003**, *21* (7), 778-84.
34. Matsumura, Y.; Ananthaswamy, H. N., Toxic effects of ultraviolet radiation on the skin. *Toxicol Appl Pharmacol* **2004**, *195* (3), 298-308.
35. Bliman, D.; Nilsson, J. R.; Kettunen, P.; Andréasson, J.; Gr?tli, M., A Caged Ret Kinase Inhibitor and its Effect on Motoneuron Development in Zebrafish Embryos. *Scientific Reports* **2015**, *5* (1), 13109.
36. Wang, Y. M.; Liu, L. Q.; Fan, S. Y.; Xiao, D.; Xie, F.; Li, W.; Zhong, W.; Zhou, X. B., Antibody-Drug Conjugate Using Ionized Cys-Linker-MMAE as the Potent Payload Shows Optimal Therapeutic Safety. *Cancers* **2020**, *12* (3).
37. Matsumura, Y.; Ananthaswamy, H. N., Toxic effects of ultraviolet radiation on the skin. *Toxicol Appl Pharm* **2004**, *195* (3), 298-308.
38. D'Orazio, J.; Jarrett, S.; Amaro-Ortiz, A.; Scott, T., UV Radiation and the Skin. *Int J Mol Sci* **2013**, *14* (6), 12222-12248.
39. Morison, W. L.; Parrish, J. A.; Fitzpatrick, T. B., Controlled study of PUVA and adjunctive topical therapy in the management of psoriasis. *Br J Dermatol* **1978**, *98* (2), 125-32.
40. Pinchuk, B.; Horbert, R.; Dobber, A.; Kuhl, L.; Peifer, C., Photoactivatable Caged Prodrugs of VEGFR-2 Kinase Inhibitors. *Molecules* **2016**, *21* (5).

- Antibody-drug conjugates are hopeful to revolutionize current cancer treatment strategies, but still restrained by off-target toxicity.
- Developing novel photocontrol-ADC to release highly active cytotoxin precisely in the tumor site upon UV irradiation seemed an attractive subject, but still challenging.
- The first ultraviolet (UV) light-controlled ADCs were designed by tactfully replacing p-aminobenzyl with UV-cleavable o-nitro-benzyl, exhibiting good photo-controllability and lower off-target toxicity.
- The present strategy may provide a new idea for future designing of ADCs and promote the development of photocontrol systems.

**Declaration of interests**

The authors declare that they have no known competing financial interests or personal relationships that could have appeared to influence the work reported in this paper.

The authors declare the following financial interests/personal relationships which may be considered as potential competing interests:

Journal Pre-proofs